IEEE Access
Multidisciplinary ⋮ Rapid Review ⋮ Open Access Journal

Received 25 August 2023, accepted 22 September 2023, date of publication 4 October 2023, date of current version 11 October 2023.

Digital Object Identifier 10.1109/ACCESS.2023.3321991

RESEARCH ARTICLE

FloreView: An Image and Video Dataset for Forensic Analysis

DANIELE BARACCHI[1,*], DASARA SHULLANI[1,*], MASSIMO IULIANI[1,2], AND ALESSANDRO PIVA[1,2], (Fellow, IEEE)

[1]Department of Information Engineering, University of Florence, 50139 Florence, Italy
[2]FORLAB, Multimedia Forensics Laboratory, PIN Scrl, 59100 Prato, Italy

Corresponding author: Daniele Baracchi (daniele.baracchi@unifi.it)

This work was supported in part by the Italian Ministry of Universities and Research (MUR) under Grant 2017Z595XS, and in part by the Defense Advanced Research Projects Agency (DARPA) under Agreement HR00112090136.

[*]Daniele Baracchi and Dasara Shullani are co-first authors.

ABSTRACT Linking a digital image or video to its originating device, or checking the content integrity still represent challenging forensic tasks. Even though several technologies based on metadata, file format, and sensor noise have been developed to address these problems, current methods are frequently made obsolete by new customized acquisition pipelines implemented by manufacturers. Therefore, to assess the performance of the available tools and push the research activity, researchers continuously need new datasets containing contents captured with recent technologies. In this paper, we present a new image and video dataset for forensic analysis. Data, acquired by the most recent acquisition devices, were collected under strictly controlled procedures designed to limit the bias induced by differences in the acquisition process between different devices. The dataset includes over 9000 media contents captured by 46 smartphones of 11 major brands. For each device, we collected at least 100 unique natural images, 30 unique natural videos, 30 flat images, and 4 flat videos. Great care has been taken in collecting data that can be used for multiple forensic tasks; moreover, images and videos have been carefully organized so that FloreView could be used by the community immediately and effortlessly. Finally, two case studies related to image source identification and video brand identification have been performed, using state-of-the-art methods, to show how the proposed dataset can be effectively used for forensic tasks.

INDEX TERMS Datasets, image analysis, image forensics, video forensics, source identification.

I. INTRODUCTION

Digital images and videos are steadily becoming the preferred means for people to share information in an immediate and effective way. In such a scenario, digital media have also become important from the perspective of the forensic and intelligence communities, for dangerous or outright illegal contents can be easily disseminated by any web user; therefore, the capability of linking a media to its source can be of paramount importance to identify the authors of specific media contents. Researchers in multimedia forensics have addressed this problem by developing multiple tools based on the digital footprints that are inevitably left on media contents by any acquisition process, and which can therefore be used to characterize the originating device. In early approaches, the effort was focused on images acquired by digital single-lens reflex and compact cameras; however, the interest quickly shifted to cameras built into smartphones, which are currently used to produce the majority of audiovisual contents available online. Each forensic technology may look at a different media aspect (such as the structure of the container of the content itself) to characterize various aspects of the originating source, which can then be combined by an analyst to get a complete picture of the origins of a media content. Therefore, it is not surprising that each forensic technique often requires the development of new image and video datasets that satisfy specific acquisition requirements.

One of the most used techniques for source device identification is the Photo Response Non Uniformity (PRNU), which is widely considered to be the most discriminating

The associate editor coordinating the review of this manuscript and approving it for publication was Wei Wang.

fingerprint capable of uniquely characterizing the acquisition device [1], [2]. This technology is based on the extraction of a sensor fingerprint from a set of reference images and a noise residual from the tested image; the two patterns are then geometrically synchronized and their similarity is assessed through an appropriate metric such as cross-correlation or the peak-to-correlation energy (PCE). Large-scale experiments highlighted that PRNU-based source identification can be performed with a negligible false attribution rate [3]. Even though this method was first applied to still images, variations of it have been developed to handle the identification of cropped and resized contents [4]. Similar approaches have also been developed to identify the source of digital videos [5]. Datasets designed to be used with this kind of methods must contain both flat and natural images captured with the same set of devices, as the former are used to extract the sensors' fingerprints while the latter are used to evaluate the performance of the attribution process.

Even though PRNU is still considered the most effective trace for the image source attribution task, a large-scale study [6] carried out on images captured by 45 recent smartphones revealed that this fingerprint uniqueness is no longer guaranteed for most brands. In fact, many models from popular manufacturers such as Huawei and Samsung exhibit a non-negligible false positive rate. However, the underlying reason for those unexpected correlation patterns among different devices cannot be ascribed to a single specific imaging technology or processing. Several preliminary studies [7], [8], [9] have been conducted to address these issues on specific devices. However, to advance the research on this matter, updated datasets comprising images and videos captured under controlled conditions using recently released device models are required.

Leveraging the fact that modern smartphones usually use the same sensor for images and videos, new methods for source identification have been explored [10]. This has resulted in the development of various forensic solutions [11], [12], [13] for different scenarios. As those methods are based on the relationships that exists between images and videos captured using the same sensor, only datasets encompassing diverse media types acquired using the same set of devices can be used in this context.

In the latest decade, researchers developed other approaches to source characterization based on the analysis of metadata, coding information, and container structure. Although this approach is not capable to distinguish the originating device, it can determine pieces of information related to the camera brand, model, operating software, and some post-processing. Initial studies focused on the image domain and led to the development of a set of features that comprise JPEG quantization tables and image resolution values [14], [15], [16]. These features proved to be effective in linking probe images to a set of devices or editing software. Further developments including Exif metadata, other coding data, and image file structure, highlighted the capability of these features to provide hints about the image life-cycle [17], [18], [19]. Meanwhile, the spread of social media networks stimulated the use of these features to characterize compression and coding differences among social platforms [20], [21], [22], [23]. Most recent works also developed provenance detectors that attempt to go beyond the last sharing and identify whether the data underwent more than one sharing operation [24], [22], [25]. Similar approaches designed for video analysis exploit the fact that contents are saved using a specific structure called container, comprising multiple streams (video, audio, subtitles), descriptors, and metadata, showing high variability for different devices and processing history [26], [27]. A formalization of the video format analysis was recently designed by exploiting the tree-shaped container structure to characterize multiple aspects of a given content, such as the source brand, the source model, and possibly the software used for editing it or the social network on which it has been shared [28], [29], [30]. Analyses based on the container have shown remarkable performance in assessing both the origin of video contents and whether they have been subjected to any kind of manipulation. On the other hand, such traces are generally overwritten by any processing [31]; therefore, these methods can only be evaluated on benchmark datasets for which a tightly controlled acquisition process has been followed.

In this paper we introduce a new dataset comprising over 9000 media samples obtained from 46 distinct smartphones, all acquired under strictly controlled conditions. All the devices have been used to capture images and videos of the same set of subjects, and all samples have been acquired under similar lightning conditions, as depicted in Figure 1. The dataset has been designed to meet the requirements of multiple forensic methods such as the aforementioned ones, so that it could be used as a common benchmark for current and future research. By way of example, the dataset could be used for: model and device source identification [3], as it contains images captured from different devices; hybrid source identification [10] and scene content image/video registration [13], as it contains, both images and videos captured with the same sensor; image/video-based localization [32], given that the same landmarks are present in multiple devices.

Moreover, as multiple, very similar versions of the same content were acquired using distinct smartphones, the dataset can be used to identify potential biases of forensic algorithms resulting from differences in image texture and brightness. This becomes particularly valuable for AI-based approaches where inherent biases may be challenging to detect due to the opaque nature of such algorithms.

The paper is structured as follow: in Section II we report the most representative image and video forensic datasets developed in the last decades, highlighting their limits and thus the need for a new dataset; in Section III we introduce FloreView, we describe how it was acquired and labeled, and how it has been organized to meet the usage needs of the forensic community; finally, in Section IV-A and Section IV-B we report two case studies related to PRNU-based image source identification and container-based video brand classification, respectively.

II. RECENT IMAGE AND VIDEO FORENSIC DATASETS

In the last decades, the research community developed several datasets to evaluate the performance of forensic solutions for source characterization tasks. Most of those datasets include both images and videos acquired in such a way as to fulfill the preconditions of a specific forensic technique or task. However, as each method has different requirements, those datasets are often unsuitable for evaluating even closely related techniques and cannot therefore be used to produce a common benchmark against which to compare different methods.

The Forchheim image database [33] is composed by more than 23000 images, including 3851 camera-native images and the corresponding versions shared on 5 social media platforms. The ACID dataset [34], in contrast, focuses on videos and includes over 12000 contents of that type captured using 46 camera models. Although videos included in this dataset are generally short (at least 5 seconds), they depict both indoor and outdoor settings, and different lighting conditions and camera movements (panning, rotating, moving forward/backward). Similarly, the Qatar University Forensic Video Database (QUFVD) [35] contains about 6000 videos from smartphones of 20 different brands. A unique feature of this dataset is that it includes exactly two models for each smartphone brand, and exactly two devices for each model. Even though these datasets include large amount of data, they cannot be used to evaluate methods that require both images and videos captured with the same sensor, as all of them only include one kind of media.

The VISION dataset [36] was designed to address this problem, consisting of images and videos from 35 portable devices of 11 brands. Overall, the dataset consists of over 34000 images and almost 2000 videos representing both outdoor and indoor scenarios. Collected images and videos have also been exchanged through three social networks (Facebook, YouTube, and WhatsApp), enabling the evaluation of available technologies on shared media. A part of the video dataset was also exchanged through a larger collection of social platforms (including Tiktok and Weibo) and manipulated using several editing applications [29]. During acquisition, however, no limits were placed on the subjects to be represented in the images and videos, and as a result there are significant differences between the contents of images and videos captured with different devices. Furthermore, VISION data were collected in 2016 and cannot therefore include contents captured using advanced imaging techniques implemented in the last few years. A similar large-scale dataset is SOCRatES [37], which includes almost 10000 images and 1000 videos from 103 smartphones of 15 different brands. Data contained in SOCRatES, however, has been acquired in the wild, resulting in both inconsistency in the subjects depicted in the acquired media and unevenness in metadata, resolution, and compression settings (e.g. 576 × 320 videos acquired with an iPhone 5). The Daxing dataset [38] is composed of 43400 images and 1400 videos captured by 90 smartphones of 22 models belonging to 5 brands only. The peculiarity of this dataset is the presence within it of contents acquired with different devices of the same model (e.g. 13 different iPhone 6S devices). It includes devices released in 2017 or before. Furthermore, the acquired contents includes a selection of subjects, such as "grass", "sky", "staircase", "lobby walls". Each subject is captured with camera default settings and the media were acquired using the smartphone under three different orientations (0°, 90°, 180°). Finally, the NYUAD mixed media dataset [39] was developed with images and videos from 78 smartphone cameras (19 brands, 62 models). Overall, the dataset includes almost 7000 images, and 301 non-stabilized videos. Since the dataset is used for focusing on the source identification when fingerprints are misaligned, attention was put to the media acquisition with different camera resolutions. No restrictions were applied to the shooting scene and limited information is shared of this dataset.

It is worth mentioning that the content of images and videos may significantly impact the performance of some methods such as the PRNU-based source identification, and thus the viability of using a dataset as a benchmark. It is well known, for instance, that the sensor fingerprint estimate is affected by content brightness and texture [2]. Therefore, in most datasets, a significant number of bright, flat images and videos (e.g. depicting skies and walls) are acquired in order to have the best image references for the extraction of the PRNU. Similarly, some datasets implement some measures to try to reduce the content bias. For instance, in Daxing [38] the acquired media have been clustered into a selection of subjects (such as sky, grass, trees). To the best of our knowledge, Dresden [40] is the only example of forensic dataset where indoor and outdoor scenes have been acquired under a controlled setting in which multiple devices acquired the same scene. The dataset, however, comprises only images and it dates back to 2010; therefore, it is not adequate to evaluate forensic techniques on modern acquisition pipelines. Such coherency among media contents, although useful to decorrelate the image content from the device, has been rarely produced in the subsequent years since the acquisition of comparable contents with all the available devices requires a considerable effort.

III. FloreView DESCRIPTION

FloreView has been created by taking into account and trying to overcome the aforementioned issues and limitations of available datasets. The dataset is composed of outdoor contents captured by 46 smartphones of 11 major brands (Apple, DOOGEE, Google, Huawei, Lenovo, LG, Motorola, OnePlus, Samsung, Sony, and Xiaomi) identified with an index from D01 to D46, as shown in Table 1. For each

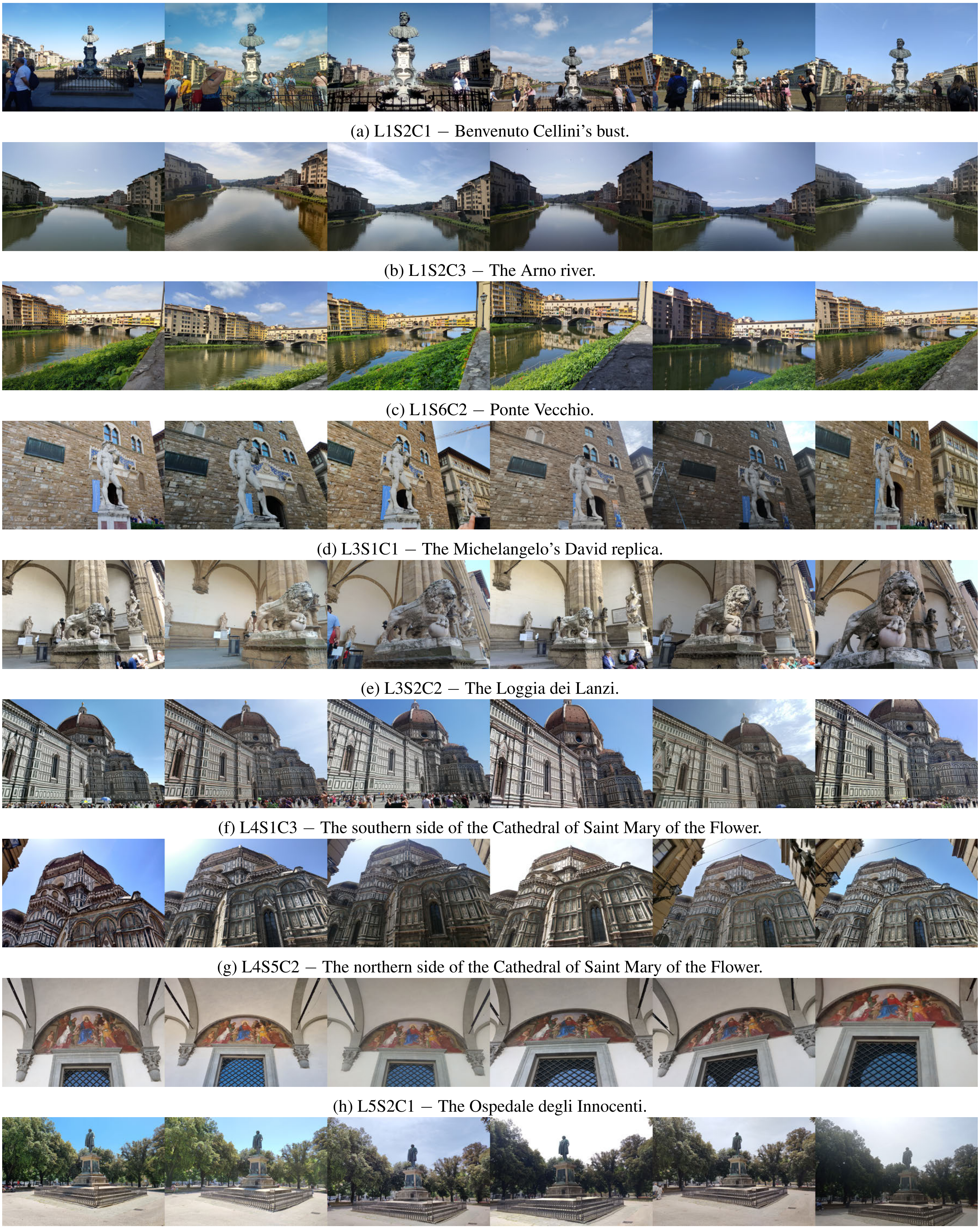

(a) L1S2C1 – Benvenuto Cellini's bust.

(b) L1S2C3 – The Arno river.

(c) L1S6C2 – Ponte Vecchio.

(d) L3S1C1 – The Michelangelo's David replica.

(e) L3S2C2 – The Loggia dei Lanzi.

(f) L4S1C3 – The southern side of the Cathedral of Saint Mary of the Flower.

(g) L4S5C2 – The northern side of the Cathedral of Saint Mary of the Flower.

(h) L5S2C1 – The Ospedale degli Innocenti.

(i) L7S4C2 – Ubaldino Peruzzi's statue.

FIGURE 1. Pictures of the same scene captured with various smartphones.

TABLE 1. Specifics of the smartphones included in FloreView. We report in columns: #iNatural the number of natural images; #vNatural the number of natural videos; #iFlat the number of flat images, and in #vFlat the number of flat videos. The number of contents with respect to the encoding algorithm are shown in columns JPEG, HEIC, H.264/AVC, and H.265/HEVC. Moreover, we report the release year for both the device (Dev.) and the firmware running on it (FW).

ID	Brand	Model name	Firmware	Release Year		#iNatural		#vNatural		#iFlat		#vFlat	
				Dev.	FW	JPEG	HEIC	H.264	H.265	JPEG	HEIC	H.264	H.265
D24	Apple	iPad Air (3rd G.)	iOS 15.5	2019	2022	106	106	36	36	35	35	5	5
D13	Apple	iPhone 8 Plus	iOS 15.4.1	2017	2022	105	-	36	-	35	-	5	-
D35	Apple	iPhone SE	iOS 15.4.1	2016	2022	108	108	36	36	41	41	5	5
D22	Apple	iPhone X	iOS 13.6	2017	2020	-	63	-	21	-	35	-	5
D02	Apple	iPhone X	iOS 15.5	2017	2022	107	107	13	36	35	35	5	5
D37	Apple	iPhone 12	iOS 15.4.1	2020	2022	107	107	36	36	35	34	5	4
D14	Apple	iPhone 13 mini	iOS 15.5	2021	2022	108	-	36	-	35	-	5	-
D27	DOOGEE	S96 Pro	Android 10	2020	2019	108	-	36	-	35	-	5	-
D19	Google	Pixel 3a	Android 12	2019	2021	108	-	36	-	36	-	5	-
D23	Google	Pixel 3a	Android 12	2019	2021	107	-	-	34	35	-	-	5
D34	Google	Pixel 5	Android 12	2020	2021	107	-	35	-	35	-	5	-
D11	Huawei	Mate 10 Lite	Android 8.0	2017	2017	107	-	36	-	34	-	5	-
D33	Huawei	Mate 10 Pro	Android 10	2017	2019	106	-	36	-	35	-	5	-
D26	Huawei	Nova 5T	Android 11	2019	2020	108	-	36	-	39	-	5	-
D03	Huawei	P8 Lite (2017)	Android 8	2017	2017	107	-	36	-	37	-	4	-
D05	Huawei	P9 Lite	Android 7	2016	2016	108	-	36	-	41	-	5	-
D12	Huawei	P30 Lite	Android 10	2019	2019	107	-	36	-	35	-	5	-
D08	Lenovo	Tab E7	Android 8.1	2018	2017	108	-	36	-	40	-	5	-
D45	LG	G4c	Android 6	2015	2015	104	-	33	-	35	-	5	-
D42	LG	G7 ThinQ	Android 10	2018	2019	108	-	36	-	41	-	5	-
D41	LG	V50 ThinQ	Android 11	2019	2020	108	-	36	-	40	-	5	-
D06	Motorola	Moto G	Android 7.1.2	2013	2016	106	-	36	-	50	-	6	-
D28	Motorola	Moto G (2nd G.)	Android 6	2014	2015	102	-	34	-	40	-	5	-
D15	Motorola	Moto G5	Android 8.1	2017	2017	107	-	36	-	35	-	5	-
D39	Motorola	Moto G5	Android 8.1	2017	2017	108	-	36	-	40	-	6	-
D29	Motorola	Moto G5S Plus	Android 8.1	2017	2017	108	-	36	-	45	-	6	-
D40	Motorola	Moto G9 Plus	Android 11	2020	2020	108	-	36	-	38	-	5	-
D21	OnePlus	6T	Android 11	2018	2020	108	-	36	-	41	-	5	-
D43	OnePlus	8T	Android 12	2020	2021	108	-	34	2	35	-	5	-
D07	Samsung	Galaxy Note 8	Android 9	2017	2018	105	-	36	-	35	-	5	-
D16	Samsung	Galaxy A12	Android 11	2020	2020	108	-	36	-	35	-	5	-
D01	Samsung	Galaxy A40	Android 11	2019	2020	107	-	36	-	41	-	4	-
D32	Samsung	Galaxy A52s (5G)	Android 12	2021	2021	108	-	36	-	35	-	5	-
D18	Samsung	Galaxy S6	Android 7	2015	2016	106	-	36	-	35	-	5	-
D44	Samsung	Galaxy S10	Android 12	2019	2021	108	-	36	-	54	-	5	-
D30	Samsung	Galaxy S10+	Android 10	2019	2019	107	-	36	-	32	-	4	-
D25	Samsung	Galaxy S20+	Android 11	2020	2020	108	-	36	-	42	-	6	-
D17	Samsung	Galaxy S21+	Android 12	2021	2021	104	-	36	-	34	-	5	-
D09	Sony	Xperia M2	Android 5.1.1	2014	2015	104	-	36	-	66	-	6	-
D31	Xiaomi	Mi A2 Lite	Android 10	2018	2019	106	-	36	-	43	-	5	-
D46	Xiaomi	Mi Mix 3	Android 10	2018	2019	104	-	34	-	35	-	5	-
D38	Xiaomi	Redmi 5 Plus	Android 8.1	2018	2017	108	-	36	-	37	-	4	-
D20	Xiaomi	Redmi Note 8	Android 9	2019	2018	108	-	36	-	35	-	5	-
D10	Xiaomi	Redmi Note 8T	Android 10	2019	2019	104	-	36	-	35	-	5	-
D04	Xiaomi	Redmi Note 8T	Android 11	2019	2020	107	-	36	-	41	-	4	-
D36	Xiaomi	Redmi Note 9	Android 11	2020	2020	107	-	36	-	40	-	5	-

smartphone, we collected at least 100 unique natural images, 30 unique natural videos, 30 flat images, and 4 flat videos, for a total of 9206 media contents (6637 images and 1831 videos). Natural images and video captured with each device depict the same subjects, in such a way as to reduce biases that might affect the performance of the analysis methods. A pictorial representation of the workflow for the acquisition process is reported in Figure 2.

A. DATA ACQUISITION CAMPAIGN

To populate the dataset, we collected images and videos of the city center of Florence (Italy). In particular, we selected 7 locations containing many famous landmarks of the city, such as `Ponte Vecchio` or the `Uffizi Gallery`. We will denote such locations as $L1, \ldots, L7$ from now on. For each location, we identified 5 subjects of interest,[1] denoted as $S1, \ldots, S5$ from now on. For instance, in `Piazza della Signoria` (L3) as depicted in Figure 3, the five chosen subjects are: *the David replica, the facade of Palazzo Vecchio, the Fountain of Neptune, the Loggia dei Lanzi, the equestrian statue of Cosimo I de' Medici.* Then, for each subject 3 images and 1 video were captured. All in all, the dataset depicts a plethora of urban areas (as shown in Figure 4) including historical buildings, statues, allies, skies, rivers, flowers, trees, people, and vehicles. For the sake of

[1] The only exception is the first location in which there are 6 subjects. That is due to the variety of scenarios offered by the location.

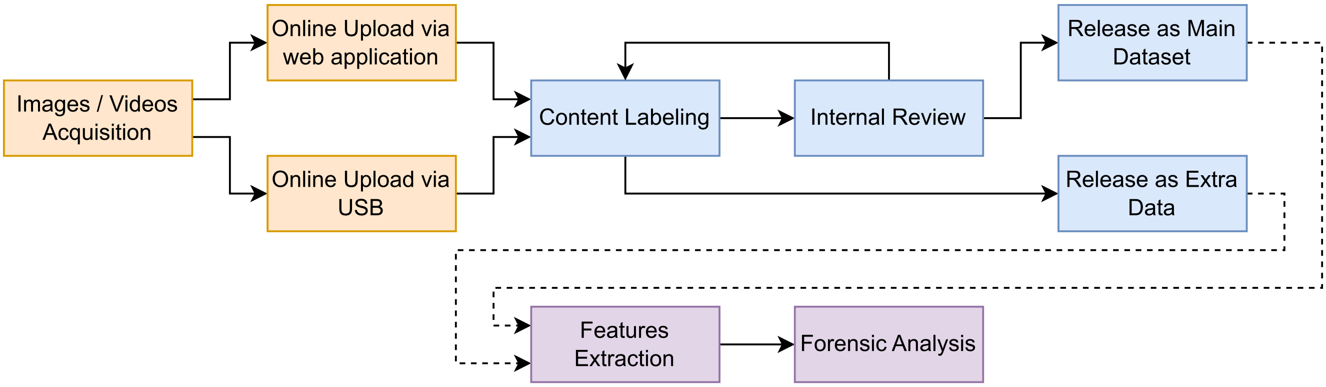

FIGURE 2. The workflow employed in creating the proposed dataset. Orange boxes represent operations performed by volunteers, blue boxes represent operations performed by the authors, and purple boxes represent operations that can be performed by the forensic community to exploit the provided data. In this paper, we carry out two experiments to illustrate the applicability of the proposed dataset for forensic purposes.

TABLE 2. A detailed list of the locations, subjects and contents available in FloreView.

Locations	Subjects	Contents

L1: Ponte Vecchio	S1: South Side;
	S2: Central;
	S3: North Side;
	S4: North-Est Side;
	S5: North-West Side;
	S6: Vasari Corridor.
		Walkway, meridian, Arno river,
		Ponte Santa Trìnita, boats, buildings.

L2: Piazzale degli Uffizi	S1: Arno Arch;
	S2: Via dei Giorgofili;
	S3: Accademia dei Giorgofili (Academy of Georgofili);
	S4: Uffizi's facade;
	S5: Uffizi Gallery.
		Memorial olive tree, Statues (Aretino, Vespucci, Galilei, Giotto, Lorenzo, Cosimo), colonnade.

L3: Piazza della Signoria	S1: David's replica;
	S2: Loggia dei Lanzi;
	S3: Palazzo Vecchio;
	S4: Fountain of Neptune;
	S5: Piazza della Signoria.
		Statues (David's replica, Abduction of a Sabine Woman, Cosimo I, lion, Perseo), Palazzo Vecchio's facade, fountain.

L4: Piazza del Duomo	S1: South-West side of Duomo;
	S2: Giotto's Campanile;
	S3: Baptistery of Saint John;
	S4: Duomo's facade;
	S5: North side of Duomo.
		Brunelleschi's Dome, Piazza di San Giovanni,
		Formelle di Andrea Pisano, Porta del Paradiso,
		Via dei Servi.

L5: Piazza della Santissima Annunziata	S1: Equestrian statue of Ferdinando I de Medici;
	S2: Ospedale degli Innocenti;
	S3: Fontana dei mostri marini (sea monster fountains);
	S4: Basilica della Santissima Annunziata (Basilica of the Most Holy Annunciation);
	S5: Basilica's portico.
		Frescos, Palazzo della Crocetta.

L6: Piazza San Marco	S1: Accademia delle Belle Arti;
	S2: Rectorate of the Università degli Studi di Firenze;
	S3: Drinking fountain;
	S4: Basilica di San Marco;
	S5: Telephone booth.
		Via Ricasoli, plaque, Madonna della Cintola,
		Manfredo Fanti's statue.

L7: Piazza dell'Indipendenza	S1: Monument to Bettino Ricasoli;
	S2: Piazza dell'Indipendenza;
	S3: Flower bed;
	S4: Ubaldino Peruzzi's statue;
	S5: Tree-lined avenue.
		Trees, relief, streetlight, city road.

clarity, in Table 2 we provide a detailed list of the contents that have been acquired.

The acquisition campaign was carried out in four mornings of late May 2022, where, for each day, contents from approximately 10 devices were collected. To provide a coherent dataset from both a content and processing chain standpoint, the settings for each smartphone were kept as uniform as feasible. Indeed, all captured data refer to the

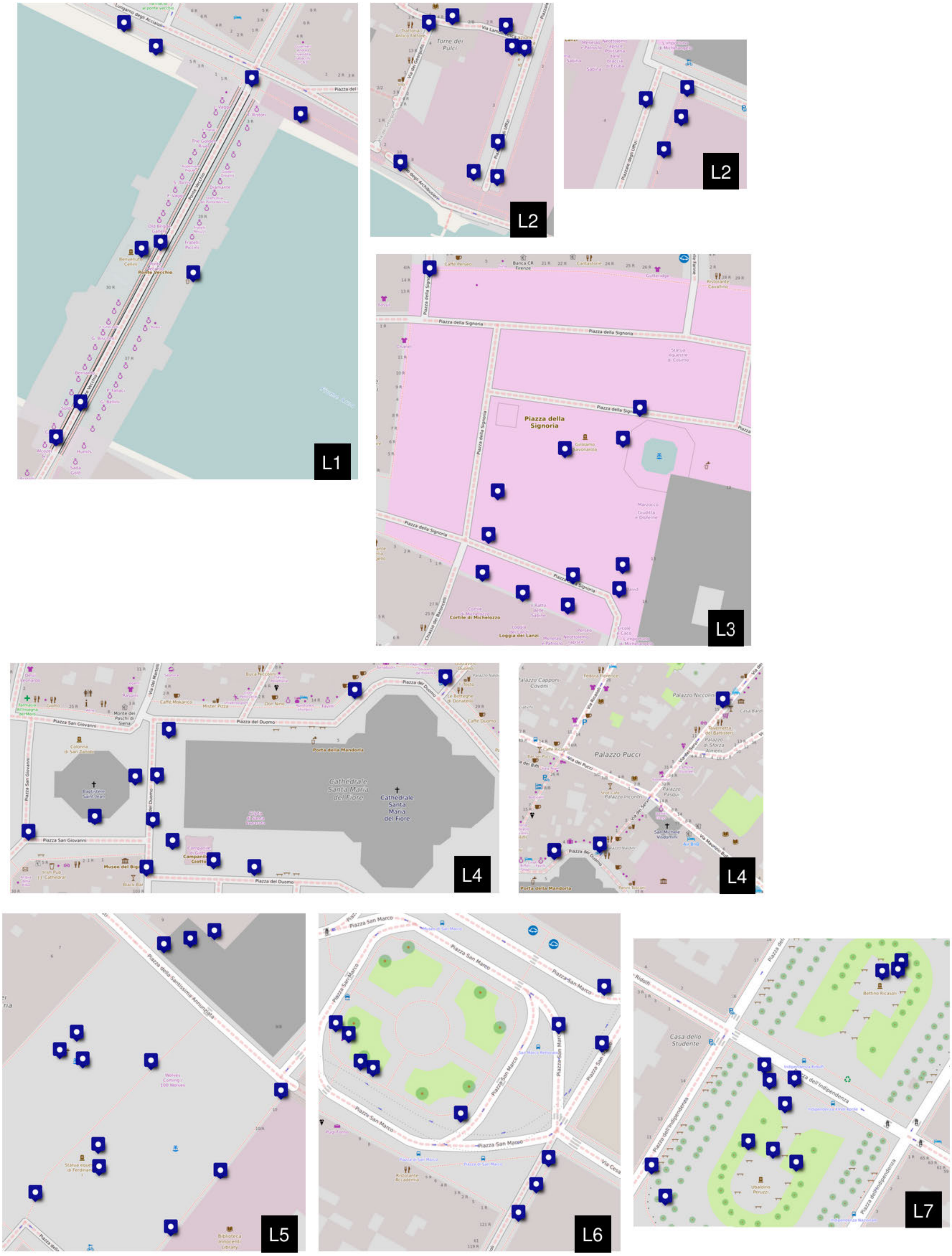

FIGURE 3. Map of locations. Ponte Vecchio (L1), Piazzale degli Uffizi (L2), Piazza della Signoria (L3), Piazza del Duomo (L4), Piazza della Santissima Annunziata (L5), Piazza San Marco (L6), Piazza dell'Indipendenza (L7). Blue-pins refer to the specific points where contents were captured.

FIGURE 4. FloreView at a glance. These are 108 natural images captured by D05, a Huawei P9 Lite.

best-quality camera available in the device; usually the one positioned on the upper rear of the smartphone. The default camera application was set to default settings, with images and videos acquired in landscape mode. Furthermore, for smartphones that permitted it, we have deactivated the EIS and HDR settings to eliminate any extra layers of processing in the acquisition pipeline. It should be noted that not all smartphones have this capability.

Each content was captured from similar points of view with every device. Depending on the location and the subject, videos were recorded in the following motion modalities: *still*, content without camera movement; *pan*, which consists of rotating the device from left to right (and vice-versa) from a fixed position; *walk*, which consists of the device moving towards the subject to acquire. We also acquired flat contents (bright blue skies) to achieve a better fingerprint estimate for source identification.

All the material has been transferred, either via wired or wireless methods, and then uploaded to an online storage website without undergoing any further post-processing.

It should be noted that Apple devices natively encode images using both the JPEG and HEIC formats and videos using both the H.264 and H.265 codecs. Therefore, it was possible to upload contents produced by 4 Apple devices twice, once for each available format.

B. LABELING SYSTEM

Given the large amount of data collected during the acquisition campaign, it has been necessary to define a robust protocol to label each image and video. For this purpose, we created a web application using the Django framework[2] to aid human experts in organizing the data. At first, contents were uploaded to different folders according to the source device and then loaded in the labeling system. The labeling system kept track of the completion status for each device, showing to each user the list of devices still needing to be processed and the percentage of labeled contents. When handling one device, the user was presented images and videos sequentially and was asked to assign, for each of them, the corresponding location, subject, and content. To reduce the chance of mislabeling, the user was able to label each content by selecting the most similar image or video from a reference set (Figure 5).

We also implemented several cross-checks to ensure the quality of assigned labels. First of all, the labeling user was asked to review their work by inspecting a final summary page showing the thumbnails for each image acquired by the device, with a chance to correct any mistakes. Moreover, in case a single content was acquired multiple times, the user had a chance to select their favourite among the duplicates (Figure 6). Then, after all the devices had been labeled, the human experts were asked to ensure that no image has been mislabeled by looking at a *content wall* depicting, for each content, a collage of all the images assigned to it (Figure 1).

Finally, labeling data was exported to multiple formats (CSV and PKL[3]) and saved along with the collected media contents.

C. DIRECTORY ORGANIZATION AND FILE NOMENCLATURE

The contents are grouped by device and organized in folders as shown in Figure 7. There are three main directories: `Flat` which contains only images and videos of skies; `Nat` which contains images and videos of natural scenes (i.e. non-flat contents); `Extra-Data` which contains images and/or videos in addition to the ones already present in the `Nat` folder. Depending on the encoding capabilities of the device, each main folder may contain either one or both of the `jpeg-h264` and `heic-h265` subdirectories.

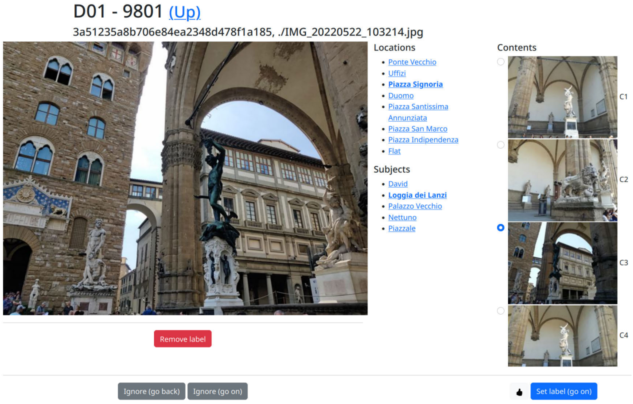

D01 - 9801 (Up)
3a51235a8b706e84ea2348d478f1a185, ./IMG_20220522_103214.jpg

FIGURE 5. A screenshot of the web application used for labelling.

The structure depicted in Figure 7 is retained in the file nomenclature. The device root directory mask name is `ID_Brand_Model`, e.g. D01_Samsung_GalaxyA40. Images and videos in `Flat` and `Nat` do not use the same convention. On the one hand, the `Flat` content mask is `ID_IXXX.ext` for images and `ID_VXXX.ext` for videos: where `ID` identifies the smartphone; `XXX` the incremental number within the image or video count; `ext` the file extension i.e. JPG/HEIC for images or MP4/3GP/MOV for videos. On the other hand, the `Nat` mask specifies the location, subject and content of the data itself.

$$\overbrace{D01}^{\text{device id}}\_\underbrace{L1}_{\text{location id}}\overbrace{S2}^{\text{subject id}}\underbrace{C1}_{\text{content id}}.\overbrace{jpeg}^{\text{file extension}}$$

In particular, content identifiers $C1$, $C2$, $C3$ correspond to images, while $C4$ identifies a video. All the duplicate labeled data that were not marked as favourites are collected into the `Extra-Data` folder, where the name mask follows the same rule used in the `Nat` directory. For instance, if we label three videos as "L2S2C4", the video `ID_L2S2C4.mp4` is stored in the path `Nat/L2/S2`, whereas videos `ID_L2S2C4_a.mp4` and `ID_L2S2C4_b.mp4` are stored in the `Extra-Data` directory.

D. DATA OVERVIEW

The devices featured in the dataset are presented in Table 1 and Table 3. Overall, 85 per cent of smartphones included in the collection run *Android OS*, while 15 per cent run *iOS*. The oldest OS release is the *Android 5.1* running on a `Sony Xperia M2`, while the latest one is the *iOS 15.5* running on an `Apple iPhone 13 mini`.

In images, the most widely used resolution in the dataset is 4032 × 3024 pixels, the highest (8000 × 6000) belongs to the `D27 DOOGEE S96 Pro`, and the lowest (1600 × 1200) belongs to the `D08 Lenovo Tab E7`. As shown in Table 1, images are stored in JPEG or HEIC formats, the former one corresponds to 91% of the images, while the latter one to the remaining 9%.

In videos, 38 out of 46 devices have a resolution of 1920 × 1080 pixels. The lowest video resolution (640 × 480)

[2] https://www.djangoproject.com/

[3] Files in PKL format are created using Python's Pickle module (https://docs.python.org/3/library/pickle.html)

TABLE 3. A summary of the characteristics of the images and videos contained in FloreView. Media duration and video frame rate values have been rounded to the nearest integer for the sake of clarity.

ID	File Type	Video Size	Media Duration (s)	Video Frame Rate	Audio Format	Compressor ID	Image Size	Rotation (°)	GPS Position
D01	[JPEG, MP4]	1920×1080	[24 – 31]	30	mp4a	avc1	4608×3456	0	No
D02	[MOV, JPEG, HEIC]	1920×1080	[25 – 30]	30	mp4a	[hvc1, avc1]	4032×3024	0	Yes
D03	[JPEG, MP4]	1280×720	[25 – 25]	29	mp4a	avc1	3840×2160	0	Yes
D04	[JPEG, MP4]	1920×1080	[25 – 26]	[29 – 30]	mp4a	avc1	4000×3000	[0, 90]	No
D05	[JPEG, MP4]	1920×1080	[22 – 26]	30	mp4a	avc1	4160×3120	0	No
D06	[JPEG, MP4]	1280×720	[22 – 26]	[29 – 30]	mp4a	avc1	2592×1944	0	No
D07	[JPEG, MP4]	1920×1080	[25 – 26]	29	mp4a	avc1	4032×3024	[0, 90]	Yes
D08	[3GP, JPEG]	640×480	[23 – 28]	[29 – 30]	mp4a	avc1	1600×1200	[0, 90]	No
D09	[JPEG, MP4]	1920×1080	[23 – 29]	[29 – 30]	mp4a	avc1	3104×1746	0	No
D10	[JPEG, MP4]	1920×1080	[24 – 26]	30	mp4a	avc1	4000×3000	0	No
D11	[JPEG, MP4]	1920×1080	[25 – 25]	30	mp4a	avc1	4608×3456	0	No
D12	[JPEG, MP4]	1920×1080	[25 – 26]	[28 – 29]	mp4a	avc1	[4000×3000, 3000×4000]	[0, 90]	Yes
D13	[MOV, JPEG]	1920×1080	[25 – 27]	30	mp4a	avc1	4032×3024	[0, 90]	No
D14	[MOV, JPEG]	1920×1080	[25 – 26]	30	mp4a	avc1	4032×3024	0	Yes
D15	[JPEG, MP4]	1280×720	[24 – 27]	[26 – 30]	mp4a	avc1	4160×2340	0	Yes
D16	[JPEG, MP4]	1920×1080	[24 – 26]	30	mp4a	avc1	4000×3000	[0, 90]	No
D17	[JPEG, MP4]	1920×1080	[25 – 26]	[30 – 60]	mp4a	avc1	4032×3024	0	No
D18	[JPEG, MP4]	1920×1080	[25 – 26]	[29 – 30]	mp4a	avc1	3264×1836	0	No
D19	[JPEG, MP4]	1920×1080	[25 – 29]	[29 – 30]	mp4a	avc1	4032×3024	0	Yes
D20	[JPEG, MP4]	1920×1080	[24 – 29]	30	mp4a	avc1	4000×3000	[0, 90]	No
D21	[JPEG, MP4]	1920×1080	[24 – 28]	[29 – 30]	mp4a	avc1	4608×2112	0	Yes
D22	[MOV, HEIC]	1920×1080	[24 – 26]	[29 – 30]	mp4a	hvc1	4032×3024	[0, 90]	Yes
D23	[JPEG, MP4]	1920×1080	[23 – 26]	[29 – 30]	mp4a	hvc1	3840×2160	0	No
D24	[MOV, JPEG, HEIC]	1280×720	[23 – 27]	29	mp4a	[hvc1, avc1]	3264×2448	0	No
D25	[JPEG, MP4]	1920×1080	[25 – 28]	[29 – 30]	mp4a	avc1	4032×3024	[0, 90]	No
D26	[JPEG, MP4]	1920×1080	[26 – 35]	29	mp4a	avc1	4000×3000	[0, 90]	No
D27	[JPEG, MP4]	3840×2160	[25 – 36]	29	mp4a	avc1	8000×6000	0	No
D28	[JPEG, MP4]	1280×720	[24 – 29]	[29 – 30]	mp4a	avc1	3264×2448	0	No
D29	[JPEG, MP4]	1920×1080	[25 – 26]	29	mp4a	avc1	4160×3120	0	No
D30	[JPEG, MP4]	1920×1080	[24 – 30]	[29 – 30]	mp4a	avc1	4032×3024	[90, 180]	Yes
D31	[JPEG, MP4]	1920×1080	[24 – 28]	[29 – 30]	mp4a	avc1	4000×3000	0	No
D32	[JPEG, MP4]	1920×1080	[25 – 31]	29	mp4a	avc1	4624×3468	0	Yes
D33	[JPEG, MP4]	1920×1080	[25 – 41]	29	mp4a	avc1	3840×2160	0	No
D34	[JPEG, MP4]	1920×1080	[22 – 28]	[31 – 60]	mp4a	avc1	[3024×4032, 4032×3024]	0	Yes
D35	[MOV, JPEG, HEIC]	1920×1080	[22 – 27]	29	mp4a	[hvc1, avc1]	4032×3024	[0, 90]	Yes
D36	[JPEG, MP4]	1920×1080	[25 – 29]	30	mp4a	avc1	4000×2992	[0, 270]	No
D37	[MOV, JPEG, HEIC]	1920×1080	[24 – 30]	29	mp4a	[hvc1, avc1]	4032 3024	[0, 90]	Yes
D38	[JPEG, MP4]	1920×1080	[24 – 27]	30	mp4a	avc1	4000×3000	0	No
D39	[JPEG, MP4]	1920×1080	[25 – 27]	[28 – 30]	mp4a	avc1	4160×3120	0	No
D40	[JPEG, MP4]	1920×1080	[22 – 31]	30	mp4a	avc1	4640×3472	0	Yes
D41	[JPEG, MP4]	1920×1080	[25 – 38]	30	mp4a	avc1	4032×3024	[0, 180]	Yes
D42	[JPEG, MP4]	1920×1080	[24 – 29]	[20 – 30]	mp4a	avc1	4656×3492	0	Yes
D43	[JPEG, MP4]	1920×1080	[25 – 31]	30	mp4a	[hvc1, avc1]	[4000×3000, 3000×4000]	0	Yes
D44	[JPEG, MP4]	1920×1080	[24 – 31]	[29 – 30]	mp4a	avc1	4032×3024	[0, 90]	No
D45	[JPEG, MP4]	1280×720	[21 – 33]	30	mp4a	avc1	[1920×1080, 3264×1840]	[0, 180]	No
D46	[JPEG, MP4]	[1920×1080, 3840×2160]	[22 – 34]	[29 – 60]	mp4a	avc1	4032×3024	[0, 180]	No

belongs to the `D08 Lenovo Tab E7`. There are three video formats in the dataset: MP4, 3GP and MOV. The first corresponds to 77% of the data, the second to 2%, and the third to 21% of the video data. As reported in Table 3, 91% of videos have a duration of 25 seconds, while the remaining 9% have a duration of at least 20 seconds. In contrast to the acquisition specifications, about 1% of videos have been acquired with a rotation of 90 degrees, and about 2% with a rotation of 180 degrees. Moreover, even though a large majority (95%) of smartphones use a frame rate of 30 fps, devices such as `D17`, `D34`, and `D46` captured videos with a frame rate of approximately 60 fps. Finally, all video contents are accompanied by an audio stream that is encoded in *mp4a* format.

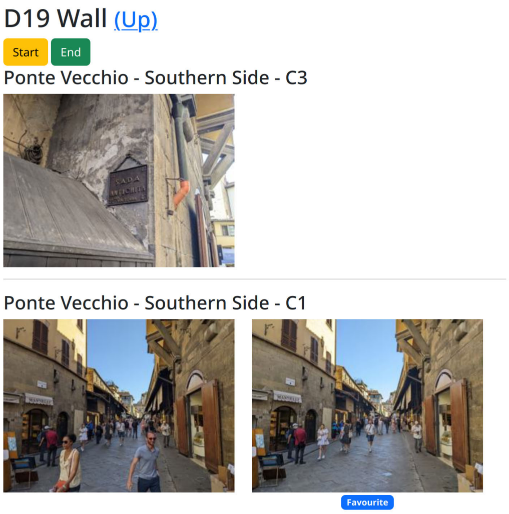
D19 Wall (Up)
Start
End
Ponte Vecchio - Southern Side - C3
Ponte Vecchio - Southern Side - C1
Favourite

FIGURE 6. **An example of the** `D19 Google Pixel 3a` **wall of contents from the labelling web application.**

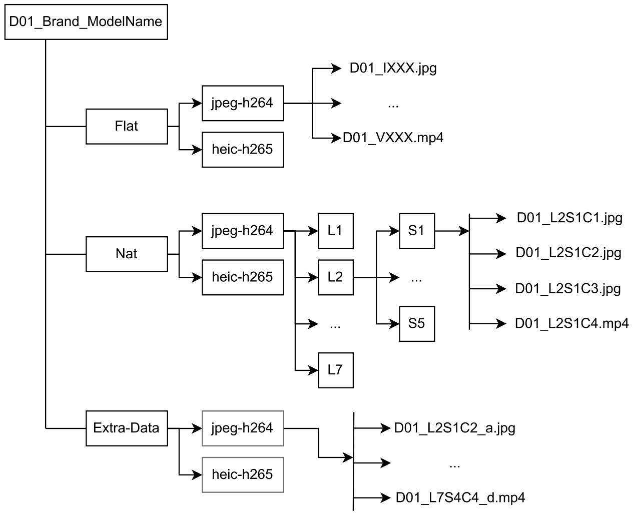

FIGURE 7. **D01 tree folder organization. Folders are depicted with a rectangular/square shape.**

E. RELEASE INFORMATION

The entire dataset is accessible at https://lesc.dinfo.unifi.it/materials/datasets_en.html, accompanied by a number of accessory files that we believe will facilitate its use by the research community. The main information released with the dataset is represented by the associated metadata, extracted via *Exiftool*[4] and *PyExif*.[5] For each device, metadata from images and videos are collected in files named `ID_[extra]_images.csv` and `ID_[extra]_videos.csv`, respectively. The identifier `[extra]` is optional, and if it is not present the metadata refers to the main dataset.

Among the many metadata found, we want to specifically mention the following: original name, orientation, brand, and model. The analysis of the original names may be relevant, for example, to trace the processing that some devices perform during a shot, such as D15's use of HDR. The Rotation (or orientation) is relevant in approaches that use the camera sensor noise to evaluate the source device, since an incorrect orientation can cause some of these methods to fail. For what concerns the brand and model, they are usually present in metadata of images and videos of Apple devices, but only in images metadata of Android devices.

In addition to data and metadata, we also make available (in pickle format) image and video features used for the experimental validation described in Section IV-A and Section IV-B as a foundation on which future researchers will be able to carry further analysis.

F. UNFORESEEABLE ASPECTS AND INCONSISTENCIES

Despite our best efforts in ensuring a uniform acquisition process, data captured by different devices may exhibit minor inconsistencies. This was mainly due to the fact that, because of the schedule of the owners of the devices, it was not possible to complete the acquisition campaign in a single day. Therefore, contents captured in different days will show traces of different transient events. For instance, traces of a political rally[6] can be found in the contents located in `Piazza Santissima Annunziata`, traces of a half-marathon can be found in data involving `the Baptistery of Saint John in Piazza del Duomo`, and traces of a statue restoration can be found in the contents of `Piazza della Signoria`. Moreover, even though we tried to avoid having faces appear in the foreground, this has proven to be difficult due to the traffic of tourists. We also report that, despite our best efforts to capture the same content at the same time on different days, we did not manage to have a perfect synchronization of the acquisition schedules, and therefore images and videos may show slight illumination differences.

A few other minor inconsistencies were found as a result of issues during the acquisition or the processing of data. Indeed, Table 1 shows some discrepancies between the number of contents captured by different devices or even between formats of the same device. For instance, there are two videos for the device `D43` that has been acquired in H.265/HEVC instead of H.264/AVC. Moreover, although the default settings of the device `D23` were activated, images were stored in JPEG format and videos encoded in H.265/HEVC. In addition, the number of natural videos belonging to the `D02` is not the same between the two codecs (13 for H.264/AVC and 36 for H.265/HEVC). Finally, the

[4] ExifTool is a platform-independent Perl library for managing metadata information for images and videos.

[5] *PyExif* is a Python wrapping for the Exiftool library.

[6] Since contents were acquired in an urban environment over which the authors had no control, political symbols and slogans may appear in the visual or audio content of the videos. The authors specify that this does not represent an endorsement on their part.

device D22 does not contain the data from all locations (four out of seven are available).

IV. FORENSIC APPLICATIONS

In this section, we address some forensics applications that can benefit from the usage of the proposed dataset. In Section IV-A we describe the exploitation of Photo Response Non-Uniformity for image source identification, and in Section IV-B we report the use of video-containers for brand identification.

A. SENSOR NOISE-BASED IMAGE SOURCE IDENTIFICATION

PRNU is a type of noise which is dominant in natural images, and is caused by the pixel-to-light sensitivity of the camera sensor [1]. This artefact, present in all images captured by the same device, makes it possible to build camera's unique fingerprint.

The camera's fingerprint $\mathbf{K}$ [2] can be estimated from J images $[\mathbf{I}_1, \ldots, \mathbf{I}_J]$ acquired by the same device by extracting their noise residuals $[\mathbf{W}_1, \ldots, \mathbf{W}_J]$ using a denoising filter [41], and then applying the maximum likelihood estimator as

$$\hat{\mathbf{K}} = \frac{\sum_{i=1}^{J} \mathbf{W}_i \mathbf{I}_i}{\sum_{i=1}^{J} \mathbf{I}_i^2}. \tag{1}$$

Finally, the estimated fingerprint $\hat{\mathbf{K}}$ is further processed to remove JPEG blocking, demosaicing traces, and other non-unique artefacts, as detailed in [1] and [2].

Given a test image $\mathbf{I}_Q$, in order to verify if its originating device is the one characterised by the estimated fingerprint $\hat{\mathbf{K}}$, the correlation between query image and fingerprint is computed. More in detail, the peak-to-correlation energy (PCE) is computed, being more advantageous than a simple correlation [3]. In particular, given the camera fingerprint estimate $\hat{\mathbf{K}}$, the query image $\mathbf{I}_Q$, and the noise residual $\mathbf{W}_Q$ extracted from $\mathbf{I}_Q$, the PCE is computed as

$$PCE = \frac{\rho(\mathbf{s}_{peak})^2}{\frac{1}{M \times N - |\mathcal{S}|} \sum_{\mathbf{s} \notin \mathcal{S}} \rho(\mathbf{s})^2} \tag{2}$$

where $\rho(\mathbf{s})$ is the two-dimensional normalized cross-correlation between the matrices $\mathbf{I}_Q\hat{\mathbf{K}}$ and $\mathbf{W}_Q$ for any valid two-dimensional shift $\mathbf{s}$; $\mathbf{s}_{peak}$ is the peak point; $\mathcal{S}$ is a small set of peak neighbours, and $M \times N$ is the image resolution. PCE ratio is thresholded to attribute the query image $\mathbf{I}_Q$ to the reference device which generated $\hat{\mathbf{K}}$. It is generally accepted that if $PCE \geq 60$, the query image can be attributed to the reference device represented by the fingerprint $\hat{\mathbf{K}}$ [3].

1) IMPLEMENTATION DETAILS AND DISCUSSION

For each smartphone in the dataset we performed the device attribution test as follows. First, a *reference fingerprint* for each device $\hat{\mathbf{K}}$ was built by exploiting Eq. 1 using [8, 16, 24, 32][7] flat images, by exploiting a Python3 implementation of a PRNU extractor[8] that generates the fingerprint and the extracted noise from a central image patch of 512 × 512 pixels.

Second, all the natural images from the same device were compared against the device fingerprint according to Eq. 2 and considered to be a *match* (True Positive) if the computed PCE is greater than or equal to 60. Third, all natural images were compared against every fingerprint in the dataset and, when the PCE exceeded the threshold on a sensor other than the original, a *mismatch* (False Positive) is recorded. We performed the same analysis on both JPEG and HEIC images.

Table 4 depicts the performance of source identification for each brand in terms of True Positive Rate (TPR), False Positive Rate (FPR) and area under the ROC curve (AUC). In particular, when the statistical feature PCE is compared to a fixed threshold equal to 60, TPR is the probability that a query image is correctly assigned to its source device, while FPR is the probability that a query image from a different source device is wrongly assigned to the one under consideration. The AUC is the area under the receiver operating characteristic (ROC) curve describing the performance of the method at all classification thresholds.

Overall, Lenovo and DOOGEE have the best performances in terms of AUC; they are also two of the three brands with only one device. The tests show that most brands have zero False Positive Rate (FPR), with the sole exception of Samsung showing a negligible value of 0.4%. In addition, an increase in the number of flat images used to compute the fingerprint corresponds to an increase in performance for both TPR (on average 14%) and AUC (on average 2%). It is worth noticing that half of such increment is achieved with 16 flat images while a further increase on the number of images do not provide a significant improvement to the reference estimate. Moreover, Xiaomi is the worst performing brand; in fact, even in the best scenario, only a little more than half of its original images can be positively matched, with an overall AUC of 0.80. This behaviour is best understood by analysing Figure 8. Indeed, one can see that half of Xiaomi devices have a nearly zero TPR (D20, D46, D10) that clearly explains the lower performances shown in Table 4. In the proposed dataset, there are 19 devices in which a TPR over 0.80 can be achieved with a fingerprint of 16 flat images, and very few cases of false alarms. It is worth noticing the behaviour of the device D36: with 16 flat images a TPR of 0.70 is obtained, but as the flats increase the TPR slightly decreases to 0.66. This is probably due to the choice of images used in the performance evaluation.

To complete the analysis, in Table 5 we provide a detailed information about the Samsung and Google devices that

[7] The maximum number of flat images is due to the availability of the D30 Samsung Galaxy S10+.

[8] The PRNU extractor by *Image and Sound Processing Lab* is available on GitHub at https://github.com/polimi-ispl/prnu-python

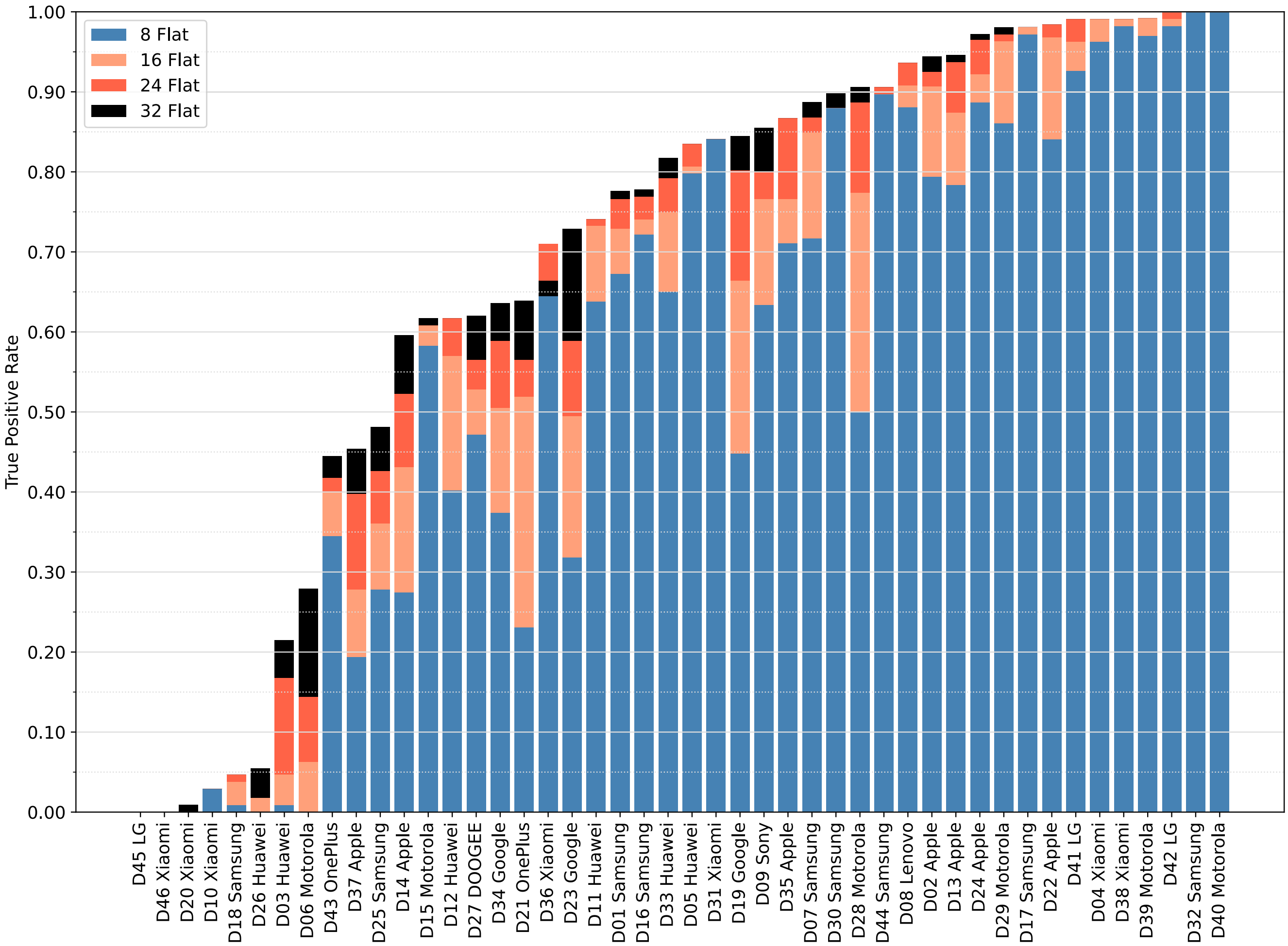

FIGURE 8. True Positive Rate per device. Fingerprints are computed with [8, 16, 24, 32] flat images, which are respectively colored in *steel*, *lightsalmon*, *tomato*, and *black*. Dotted lines in *gray* represent TPR values at intervals of 0.05.

TABLE 4. Performance of sensor noise-based image source identification [3] in terms of: TPR - True Positive Rate and FPR - False positve rate with a PCE threshold of 60; AUC - Area under the ROC curve, computed for varying PCE thresholds. Best results are depicted in bold and *italic*. Worst results are underlined.

Brand	nDevs	8 Flat			16 Flat			24 Flat			32 Flat		
		TPR	FPR	AUC	TPR	FPR	AUC	TPR	FPR	AUC	TPR	FPR	AUC
Samsung	9	**0.69**	<0.01	0.89	0.72	<0.01	0.91	0.74	<0.01	0.93	0.75	<0.01	0.92
Apple	7	0.64	-	**0.94**	0.73	-	**0.95**	**0.80**	-	**0.97**	**0.82**	-	**0.98**
Huawei	6	0.42	-	0.85	0.50	-	0.86	0.54	-	0.87	0.55	-	0.88
Xiaomi	6	0.54	-	0.80	0.55	-	0.79	0.54	-	0.80	0.54	-	0.80
Motorola	6	0.66	-	0.93	**0.74**	-	0.95	0.77	-	0.96	0.80	-	0.96
Google	3	0.38	-	0.93	0.56	-	0.95	0.66	-	0.97	0.74	-	0.98
LG	3	0.62	-	0.82	0.63	-	0.84	0.65	-	0.84	0.65	-	0.82
OnePlus	2	0.29	-	0.84	0.46	-	0.87	0.49	-	0.89	0.54	-	0.89
Lenovo	1	*0.88*	-	*0.99*	*0.91*	-	*0.99*	*0.94*	-	*0.99*	*0.94*	-	0.98
Sony	1	0.63	-	0.93	0.77	-	0.96	0.80	-	0.97	0.85	-	0.97
DOOGEE	1	0.47	-	*0.99*	0.53	-	*0.99*	0.56	-	*0.99*	0.62	-	*0.99*

expose a non-negligible FPR.[9] The column *#Fingerprint* shows the camera's fingerprint that wrongly matches with some images of the device described in the columns *ID*, *Brand*, and *Model*. The column *#Mis. Images* refers to the number of mismatching images (i.e. giving a false positive) with respect to the total number of images of that device,

[9] For ease of presentation, we only show results with 32 flats, but similar mismatch performances are obtained when the fingerprint is built with only 8 flat images. Moreover, the FPR value for the Google devices is not shown in Table 4, due to its very low value.

TABLE 5. Details about devices that expose a non-null FPR when using fingerprints built with 32 flat images. *#Fingerprint* shows the camera's fingerprint that wrongly matches with some images of the device identified by *ID*, *Brand*, and *Model*. *#Mis. Images* refers to the number of mismatching images with respect to the total number of *#Images* of that device.

Fingerprint	Devices' mismatches				
	ID	Brand	Model	#Images	#Mis. Images
D30 Samsung Galaxy S10+	D17	Samsung	Galaxy S21+	104	2
	D44	Samsung	Galaxy S10	108	102
D44 Samsung Galaxy S10	D17	Samsung	Galaxy S21+	104	2
	D30	Samsung	Galaxy S10+	107	94
D19 Google Pixel 3a	D34	Google	Pixel 5	108	2
D42 LG G7 ThinQ	D32	Samsung	Galaxy A52s (5G)	108	2

given in *#Images*. The fingerprint of the D30 Samsung Galaxy S10+ obtained a high PCE value when compared to the residual noise of 2 images of the D17 Samsung Galaxy S21+, and 102 images of the D44 Samsung Galaxy S10. 87% of natural images captured by D30 do match the D44 fingerprint, and 94% of natural images captured by D44 do match the D30 fingerprint. These results support the behaviour observed by Iuliani et al. [6], where pictures from Samsung Galaxy S10 have many collisions even if compared with different sensors but of the same brand and model. In Figure 9 and Table 5 we provide fingerprints comparisons between devices showing mismatches. Interestingly, a high correlation is found between two couple of devices (D30–D44 and D19–D34), suggesting that there are some non-unique artefacts that are not removed through the estimation process employed by the state of the art. Conversely, false alarms generated from images belonging to D17 and D32 devices can be reasonably attributed to statistical anomalies.

B. CONTAINER-BASED VIDEO BRAND IDENTIFICATION

When a camera acquires a digital video, the visual and audio streams are encoded in parallel. After compression and synchronization, the streams are encapsulated in a multimedia container, simply called a video container from now on. Nowadays, most smartphones capture videos in *MOV*, *MP4*, or *3GP* formats, all of them storing the content according to the *ISO Base format* standard. The standard describes the video format as a tree structure in which nodes may be either mandatory or optional. Optional elements allow various brands to customize the structure of the produced videos, albeit with the consequence of leaving behind forensic traces. By analysing this standard, Iuliani et al. [28] proposed a way to formalize a video container V as a set of symbols $\{s_1, \dots s_m\}$, where s_i is either a *field-symbol* or a *value-symbol*. The former corresponds to the path from the root to any field (value excluded), and the latter corresponds to the path from the root to any field-value (value included).

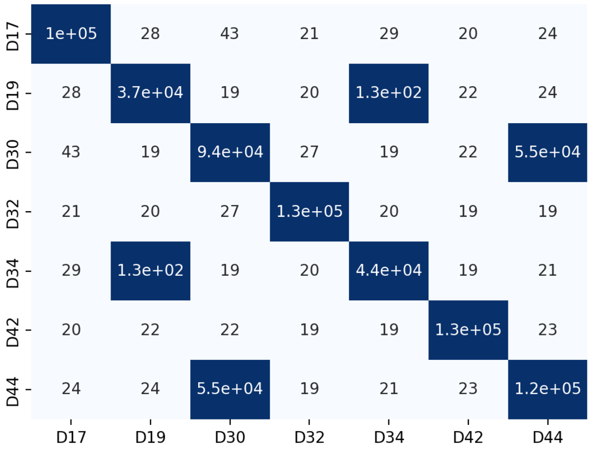

	D17	D19	D30	D32	D34	D42	D44
D17	1e+05	28	43	21	29	20	24
D19	28	3.7e+04	19	20	1.3e+02	22	24
D30	43	19	9.4e+04	27	19	22	5.5e+04
D32	21	20	27	1.3e+05	20	19	19
D34	29	1.3e+02	19	20	4.4e+04	19	21
D42	20	22	22	19	19	1.3e+05	23
D44	24	24	5.5e+04	19	21	23	1.2e+05

FIGURE 9. PCE [3] values for fingerprints comparisons between devices with 32 flat images. Values greater than 60 are colored in *dark blue*.

An example [10] is the following:

$$s_1 = [\texttt{ftyp/@majorBrand}]$$
$$s_2 = [\texttt{ftyp/@majorBrand/qt}]$$
$$s_3 = [\texttt{ftyp/@compatibleBrand\_1/qt}]$$
$$\dots$$
$$s_i = [\texttt{moov/mvhd/@volume}]$$
$$s_{i+1} = [\texttt{moov/mvhd/@volume/1.0}]$$
$$\dots$$

Given $\mathcal{O} = \{O_1, \dots, O_n\}$ a set of possible origins (e.g. different brands), the container V can be assigned to a specific class O_i based on its symbols $\{s_1, \dots, s_m\}$ by its comparison with representative containers of each class. This method was further improved by Yang et al. [29], who proposed an efficient way to analyze video file containers independently on the reference dataset's size by exploiting Decision Trees.

1) IMPLEMENTATION DETAILS AND DISCUSSION

Brand identification has been performed on available data by means of a leave-one-device-out cross validation, in which each fold consists of examples belonging to one smartphone. Brands with only one device were left out from the analysis, resulting in an evaluation of 8 brands.

We employed the methodology presented in Yang et al. [29], which constructs a set of representative symbols for each trained brand. These symbols are then utilized to classify the symbols found in the tested videos using a decision tree. In Table 6 we report the results of the brand identification in terms of classification accuracy by means of a confusion matrix. Figures highlight that the performance strongly depends on the considered class. Perfect accuracy is attained in classifying videos of the brands Samsung, Google, LG, Huawei, and Apple, thanks to the high discriminating ability of their containers

[10] Note that @ is used to identify atom parameters.

TABLE 6. Classification accuracy on video identification of videos by means of video-container analysis [29]. Values in the diagonal represent the correct classification for each brand.

		Predicted Brand							
		OnePlus	Samsung	Xiaomi	Google	Motorola	LG	Huawei	Apple
True Brand	OnePlus	**0.01**	-	0.48	-	0.48	-	0.03	-
	Samsung	-	**1.00**	-	-	-	-	-	-
	Xiaomi	0.44	-	**0.00**	-	0.47	-	0.08	-
	Google	-	-	-	**1.00**	-	-	-	-
	Motorola	0.17	-	-	-	**0.83**	-	-	-
	LG	-	-	-	-	-	**1.00**	-	-
	Huawei	-	-	-	-	-	-	**1.00**	-
	Apple	-	-	-	-	-	-	-	**1.00**

in identifying their respective manufacturers. Conversely, `OnePlus`, `Xiaomi`, and `Motorola` classes share portions of the container structure, which are consequently predicted in the same group, as already noted by Iuliani et al. [28]. Indeed, a plurality of videos produced by `OnePlus` and `Xiaomi` are incorrectly attributed to `Motorola`. Ultimately, the PRNU analysis for images and the container structure analysis for videos yield the poorest results in accurately characterizing the source in `Xiaomi` devices.

V. CONCLUSION

We presented FloreView, a new image and video dataset for forensic analysis, with a special focus to brand, model, and device classification. Overall, we collected over 9000 images and videos using 46 smartphones of 11 major brands. Contents were acquired following a tightly controlled protocol to limit the biases that may be introduced by the acquisition pipeline, including camera settings and content downloads. Moreover, special care has been taken to ensure that images and videos from all the devices depicted similar scenes and subjects. The acquired data were carefully organized so that they could be used by the forensic community immediately and effortlessly. To demonstrate how our dataset can be applied in a forensic context, we conducted two case studies focused on identifying image sources and video brands. Experiments show that FloreView can be effectively used to evaluate the performance of forensic methods. The dataset is structured in such a way to allow a broad range of forensic scenarios. In addition to conventional applications such as source attribution, the fact that contents depict similar scenes opens the door to intriguing new endeavours at the crossroad of multimedia forensics and computer vision such as the automatic detection of weather conditions and crowd presence assessment.

ACKNOWLEDGMENT

The authors would like to thank the people involved in data collection: Chiara Albisani, Alberto Arienzo, Francesco Baffa, Francesco Barbieri, Alice Cavaliere, Guido Ciapetti, Andrea Cimbalo, Andrea Croce, Andrea Desideri, Carolina Di Quinzio, Elia Ducceschi, Francesco Fantechi, Yoshihisa Furushita, Lucia Giorgi, Simone Izzo, Graziano Manduzio, Stefano Martina, Elio Marunti, Lorenzo Massai, Maria Teresa Nardoni, Daniele Narducci, Alessandro Nozzoli, Simone Pezzulla, Edoardo Putti, Claudia Raffaelli, Maria Scarano, Tomaso Trinci, Alessandro Ugolini, Xingyi Yu, and Riccardo Zucchini.

The U.S. government is authorized to reproduce and distribute reprints for Governmental purposes notwithstanding any copyright notation thereon. The views and conclusions contained herein are those of the authors and should not be interpreted as necessarily representing the official policies or endorsements, either expressed or implied, of the Defense Advanced Research Projects Agency or the U.S. government.

REFERENCES

[1] J. Lukas, J. Fridrich, and M. Goljan, "Digital camera identification from sensor pattern noise," *IEEE Trans. Inf. Forensics Security*, vol. 1, no. 2, pp. 205–214, Jun. 2006.

[2] M. Chen, J. Fridrich, M. Goljan, and J. Lukas, "Determining image origin and integrity using sensor noise," *IEEE Trans. Inf. Forensics Security*, vol. 3, no. 1, pp. 74–90, Mar. 2008.

[3] M. Goljan, J. Fridrich, and T. Filler, "Large scale test of sensor fingerprint camera identification," *Proc. SPIE*, vol. 7254, Feb. 2009, pp. 170–181.

[4] M. Goljan and J. Fridrich, "Camera identification from cropped and scaled images," *Proc. SPIE*, vol. 6819, pp. 154–166, Mar. 2008.

[5] M. Chen, J. Fridrich, M. Goljan, and J. Lukáš, "Source digital camcorder identification using sensor photo response non-uniformity," *Proc. SPIE*, vol. 6505, pp. 517–528, Mar. 2007.

[6] M. Iuliani, M. Fontani, and A. Piva, "A leak in PRNU based source identification—Questioning fingerprint uniqueness," *IEEE Access*, vol. 9, pp. 52455–52463, 2021.

[7] C. Albisani, M. Iuliani, and A. Piva, "Checking PRNU usability on modern devices," in *Proc. IEEE Int. Conf. Acoust., Speech Signal Process. (ICASSP)*, Jun. 2021, pp. 2535–2539.

[8] D. Baracchi, M. Iuliani, A. G. Nencini, and A. Piva, "Facing image source attribution on iPhone X," in *Proc. Int. Workshop Digit. Watermarking*, Melbourne, VIC, Australia: Springer, Nov. 2020, pp. 196–207.

[9] N. Nisar Bhat and T. Bianchi, "Investigating inconsistencies in PRNU-based camera identification," in *Proc. IEEE Int. Conf. Image Process. (ICIP)*, Oct. 2022, pp. 851–855.

[10] M. Iuliani, M. Fontani, D. Shullani, and A. Piva, "Hybrid reference-based video source identification," *Sensors*, vol. 19, no. 3, p. 649, Feb. 2019.

[11] S. Mandelli, F. Argenti, P. Bestagini, M. Iuliani, A. Piva, and S. Tubaro, "A modified Fourier–Mellin approach for source device identification on stabilized videos," in *Proc. IEEE Int. Conf. Image Process. (ICIP)*, Oct. 2020, pp. 1266–1270.

[12] P. Ferrara, M. Iuliani, and A. Piva, "PRNU-based video source attribution: Which frames are you using?" *J. Imag.*, vol. 8, no. 3, p. 57, Feb. 2022.

[13] F. Bellavia, M. Fanfani, C. Colombo, and A. Piva, "Experiencing with electronic image stabilization and PRNU through scene content image registration," *Pattern Recognit. Lett.*, vol. 145, pp. 8–15, May 2021.

[14] H. Farid, "Digital image ballistics from jpeg quantization," Dept. Comput. Sci., Dartmouth College, Hanover, NH, USA, Tech. Rep. TR9-1-2006, 2006.

[15] J. D. Kornblum, "Using JPEG quantization tables to identify imagery processed by software," *Digit. Invest.*, vol. 5, pp. S21–S25, Sep. 2008. [Online]. Available: https://www.sciencedirect.com/science/article/pii/S1742287608000285

[16] H. Farid, "Digital image ballistics from JPEG quantization: a followup study," Dept. Comput. Sci., Dartmouth College, Hanover, NH, USA, Tech. Rep. TR2008–638, 2008.

[17] E. Kee, M. K. Johnson, and H. Farid, "Digital image authentication from JPEG headers," *IEEE Trans. Inf. Forensics Security*, vol. 6, no. 3, pp. 1066–1075, Sep. 2011, doi: 10.1109/TIFS.2011.2128309.

[18] T. Gloe, "Forensic analysis of ordered data structures on the example of JPEG files," in *Proc. IEEE Int. Workshop Inf. Forensics Secur. (WIFS)*, Tenerife, Spain, Dec. 2012, pp. 139–144, doi: 10.1109/WIFS.2012.6412639.

[19] P. Mullan, C. Riess, and F. Freiling, "Forensic source identification using JPEG image headers: The case of smartphones," *Digit. Invest.*, vol. 28, pp. S68–S76, Apr. 2019. [Online]. Available: https://www.sciencedirect.com/science/article/pii/S174228761930026X

[20] A. Castiglione, G. Cattaneo, and A. De Santis, "A forensic analysis of images on online social networks," in *Proc. 3rd Int. Conf. Intell. Netw. Collaborative Syst.*, Nov. 2011, pp. 679–684.

[21] O. Giudice, A. Paratore, M. Moltisanti, and S. Battiato, "A classification engine for image ballistics of social data," in *Image Analysis and Processing ICIAP 2017*, S. Battiato, G. Gallo, R. Schettini, and F. Stanco, Eds. Cham, Switzerland: Springer, 2017, pp. 625–636.

[22] Q. Phan, G. Boato, R. Caldelli, and I. Amerini, "Tracking multiple image sharing on social networks," in *Proc. IEEE Int. Conf. Acoust., Speech Signal Process. (ICASSP)*, May 2019, pp. 8266–8270.

[23] S. Magistri, D. Baracchi, D. Shullani, A. D. Bagdanov, and A. Piva, "Towards continual social network identification," in *Proc. 11th Int. Workshop Biometrics Forensics (IWBF)*, Apr. 2023, pp. 1–6.

[24] Q.-T. Phan, C. Pasquini, G. Boato, and F. G. B. De Natale, "Identifying image provenance: An analysis of mobile instant messaging apps," in *Proc. IEEE 20th Int. Workshop Multimedia Signal Process. (MMSP)*, Aug. 2018, pp. 1–6.

[25] S. Verde, C. Pasquini, F. Lago, A. Goller, F. De Natale, A. Piva, and G. Boato, "Multi-clue reconstruction of sharing chains for social media images," *IEEE Trans. Multimedia*, early access, Mar. 6, 2023, doi: 10.1109/TMM.2023.3253389.

[26] T. Gloe, A. Fischer, and M. Kirchner, "Forensic analysis of video file formats," *Digit. Invest.*, vol. 11, pp. S68–S76, May 2014.

[27] D. Güera, S. Baireddy, P. Bestagini, S. Tubaro, and E. J. Delp, "We need no pixels: Video manipulation detection using stream descriptors," 2019, *arXiv:1906.08743*.

[28] M. Iuliani, D. Shullani, M. Fontani, S. Meucci, and A. Piva, "A video forensic framework for the unsupervised analysis of MP4-like file container," *IEEE Trans. Inf. Forensics Security*, vol. 14, no. 3, pp. 635–645, Mar. 2019.

[29] P. Yang, D. Baracchi, M. Iuliani, D. Shullani, R. Ni, Y. Zhao, and A. Piva, "Efficient video integrity analysis through container characterization," *IEEE J. Sel. Topics Signal Process.*, vol. 14, no. 5, pp. 947–954, Aug. 2020.

[30] E. Altinisik, H. T. Sencar, and D. Tabaa, "Video source characterization using encoding and encapsulation characteristics," *IEEE Trans. Inf. Forensics Security*, vol. 17, pp. 3211–3224, 2022.

[31] D. Shullani, D. Baracchi, M. Iuliani, and A. Piva, "Social network identification of laundered videos based on DCT coefficient analysis," *IEEE Signal Process. Lett.*, vol. 29, pp. 1112–1116, 2022.

[32] C. Masone and B. Caputo, "A survey on deep visual place recognition," *IEEE Access*, vol. 9, pp. 19516–19547, 2021.

[33] B. Hadwiger and C. Riess, "The Forchheim image database for camera identification in the wild," in *Proc. Int. Conf. Pattern Recognit.* Cham, Switzerland: Springer, 2021, pp. 500–515.

[34] B. C. Hosler, X. Zhao, O. Mayer, C. Chen, J. A. Shackleford, and M. C. Stamm, "The video authentication and camera identification database: A new database for video forensics," *IEEE Access*, vol. 7, pp. 76937–76948, 2019.

[35] Y. Akbari, S. Al-Maadeed, N. Al-Maadeed, A. A. Najeeb, A. Al-Ali, F. Khelifi, and A. Lawgaly, "A new forensic video database for source smartphone identification: Description and analysis," *IEEE Access*, vol. 10, pp. 20080–20091, 2022.

[36] D. Shullani, M. Fontani, M. Iuliani, O. A. Shaya, and A. Piva, "VISION: A video and image dataset for source identification," *EURASIP J. Inf. Secur.*, vol. 2017, no. 1, pp. 1–16, Dec. 2017.

[37] C. Galdi, F. Hartung, and J.-L. Dugelay, "SOCRatES: A database of realistic data for SOurce camera REcognition on smartphones," in *Proc. 8th Int. Conf. Pattern Recognit. Appl. Methods*, 2019, pp. 648–655.

[38] H. Tian, Y. Xiao, G. Cao, Y. Zhang, Z. Xu, and Y. Zhao, "Daxing smartphone identification dataset," *IEEE Access*, vol. 7, pp. 101046–101053, 2019.

[39] S. Taspinar, M. Mohanty, and N. Memon, "Camera identification of multi-format devices," *Pattern Recognit. Lett.*, vol. 140, pp. 288–294, Dec. 2020.

[40] T. Gloe and R. Böhme, "The 'Dresden image database' for benchmarking digital image forensics," in *Proc. ACM Symp. Appl. Comput.*, Mar. 2010, pp. 1584–1590.

[41] M. K. Mihcak, I. Kozintsev, and K. Ramchandran, "Spatially adaptive statistical modeling of wavelet image coefficients and its application to denoising," in *Proc. IEEE Int. Conf. Acoust., Speech, Signal Process. (ICASS)*, Mar. 1999, pp. 3253–3256.

DANIELE BARACCHI received the bachelor's and master's degrees in computer engineering and the Ph.D. degree in information engineering from the University of Florence. He is currently a Postdoctoral Fellow with the University of Florence, where he has been a member of the Image Analysis, Processing, and Protection Research Group, Department of Information Engineering, since 2018. In this role, he is actively engaged in the development of machine learning-based techniques for multimedia forensics. Over the past four years, he has contributed to research initiatives supported by both the U.S. Defense Advanced Research Projects Agency (DARPA) and the Italian Ministry of University and Research (MUR).

DASARA SHULLANI received the master's degree in computer engineering from Politecnico di Torino and the Ph.D. degree in information engineering from the University of Florence. Since 2015, she has been a member of the Image Analysis, Processing, and Protection Research Group, Department of Information Engineering, University of Florence, where she is developing multimedia forensics tools applied to video contents. She is currently a Postdoctoral Fellow with the University of Florence. During this period, she has worked on research projects funded by the Consortium GARR, the U.S. Defence Advanced Research Project Agency (DARPA), and the Italian Ministry of University and Research (MUR).

MASSIMO IULIANI received the master's degree in applied mathematics from the University of Florence. He is currently a Postdoctoral Fellow with the University of Florence. He also works with the Image Analysis Processing and Protection Group, Department of Information Engineering, University of Florence. In the last seven years, he worked on research projects funded by the European Commission (EC) and the U.S. Defense Advanced Research Projects Agency (DARPA). All projects were related to authentication and reverse engineering of multimedia contents. He is also a Technical Supervisor with FORLAB, Multimedia Forensics Laboratory, University of Florence. His main activities involve the training of law enforcement and legal operators and the consultancy multimedia contents analysis (digital images, audio, and videos) for forensic purposes.

ALESSANDRO PIVA (Fellow, IEEE) is currently an Associate Professor with the Department of Information Engineering, University of Florence, where he is also the Head of FORLAB—Multimedia Forensics Laboratory. His research interests include information forensics and security, of image and video processing, data hiding, signal processing in the encrypted domain, image, video forensic techniques, the design of image and video processing and analysis techniques for cultural heritage, medical, and industrial applications. In the above research topics, he has been the coauthor of more than 50 papers published in international journals and 120 papers published in international conference proceedings, with H-index 40 according to Scopus.

Open Access funding provided by 'Università degli Studi di Firenze' within the CRUI CARE Agreement